

promoting access to White Rose research papers



Universities of Leeds, Sheffield and York
<http://eprints.whiterose.ac.uk/>

This is an author produced version of a paper published in **Proceedings of the Institution of Mechanical Engineers, Part B: Journal of Engineering Manufacture**.

White Rose Research Online URL for this paper:
<http://eprints.whiterose.ac.uk/id/eprint/76963>

Published paper

Wang, L, Long, H, Ashley, D, Roberts, M and White, P (2011) *Effects of the roller feed ratio on wrinkling failure in conventional spinning of a cylindrical cup*. Proceedings of the Institution of Mechanical Engineers, Part B: Journal of Engineering Manufacture, 225 (11), pp. 1991 – 2006.

<http://dx.doi.org/10.1177/0954405411396024>

Effects of Roller Feed Ratio on Wrinkling Failure in Conventional Spinning of a Cylindrical Cup

L. Wang¹, H. Long^{1*}, D. Ashley², M. Roberts² and P. White²

¹School of Engineering and Computing Sciences, Durham University, Durham, United Kingdom

²Metal Spinners Group Limited, Newcastle, United Kingdom

*Corresponding author, new email: h.long@sheffield.ac.uk

The manuscript was received on 13 September 2010 and was accepted after revision for publication on 8 December 2010.

DOI: 10.1177/0954405411396024

Abstract

In this study, wrinkling failure in conventional spinning of a cylindrical cup has been investigated by using both Finite Element (FE) analysis and experimental methods. FE simulation models of a spinning experiment have been developed using the explicit finite element solution method provided by software Abaqus. The severity of wrinkles is quantified by calculating the standard deviation of the radial coordinates of element nodes on the edge of the workpiece obtained from the FE models. The results show that the severity of wrinkles tends to increase when increasing the roller feed ratio. A forming limit study for wrinkling has been carried out and it shows there is a feed ratio limit beyond which the wrinkling failure will take place. Provided that the feed ratio is kept below this limit, the wrinkling failure can be prevented. It is believed that high compressive tangential stresses in the local forming zone are the causes of the wrinkling failure. Furthermore, the computational performance of the solid and shell elements in simulating the spinning process are examined, the tool forces obtained from wrinkling and wrinkle-free models are compared. Finally the effects of the feed ratio on variations of the wall thickness of the spun cylindrical cup are investigated.

Keywords: Conventional metal spinning; Formability limit; Wrinkling failure; Finite Element analysis.

1. Introduction

Sheet metal spinning is commonly known as a metal forming process by which a flat metal sheet is rotated at a high speed and formed into an axially symmetric part by a roller which progressively forces the metal sheet onto a mandrel, as shown in Figure 1. Due to the inherent advantages of the spinning process, such as low forming load, simple tooling, good surface finish and improved mechanical properties of spun parts, metal spinning has

been increasingly used to produce components for automotive, aerospace, medical, construction and defence industries in recent years. The spinning process is capable of deforming the workpiece of sheet thickness from 0.5 mm to 30 mm and diameter of 10 mm - 5000 mm [1]. Materials used in the spinning process include non-alloyed carbon steels, heat-resistant and stainless steels, non-ferrous heavy metals and light alloys. Sheet metal spinning can be divided into two categories: shear forming and conventional spinning. Shear forming produces a desired shape by one roller pass over a metal sheet, the sheet thickness is deliberately decreased and the diameter of the workpiece remains constant during the process. In contrast, in conventional spinning, a metal sheet is deformed into a desired shape by multiple roller passes to maintain the sheet thickness unchanged but to deliberately decrease the diameter.

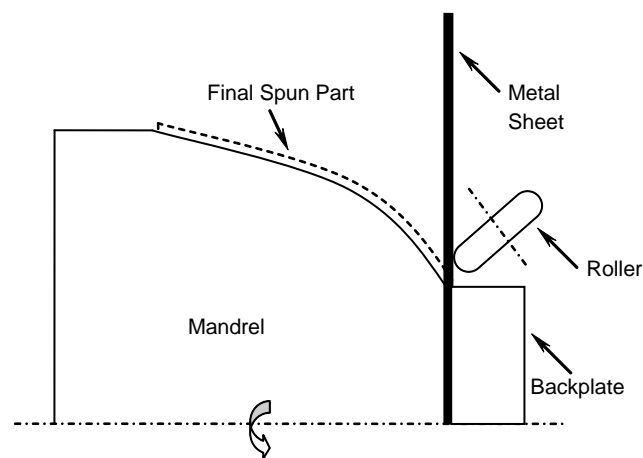


Figure 1 Illustration of conventional metal spinning process

There are three types of common material failures in the conventional spinning process [1]: wrinkling, circumferential cracking and radial cracking. Fig. 2 shows a wrinkling spun part and a wrinkling-free spun part. Wrinkling is caused by buckling effects of the unsupported flange of the metal sheet during spinning. Once the compressive tangential stress in the workpiece exceeds a buckling stability limit, wrinkling will occur. Therefore, multiple roller passes are generally required in order to keep the compressive tangential stress below the buckling limit. In the spinning process, excessive stresses in either radial or tangential direction of the spun part are undesirable.



Figure 2 Wrinkling failure in conventional spinning

As one of the main failure modes in the spinning process, wrinkling significantly affects the production efficiency and material formability. In the spinning industry, due to the lack of in-depth understanding of the failure mechanism, the process design highly relies on experienced spinners who use trial-and-error methods to avoid wrinkling failure. Few investigations on the wrinkling failures of the spinning process have been carried out in an effort to understand causes of wrinkling. However, there is limited research in developing effective means to predict and to prevent wrinkling failures by controlling process variables.

Kleiner et al [2] suggested that the wrinkling in the spinning process was not only caused by static buckling but also influenced or even triggered by the dynamic effects from the feeding of roller and the rotation of workpiece. Klimmek et al [3] suggested that investigating the stress distribution in the workpiece, especially within the local forming zone was essential in order to understand the cause of the wrinkling failure. Based on FE analysis results, Sebastiani et al [4] found a toothed stress pattern after a backward roller pass and the authors believed that it was a pre-state leading to the wrinkling failure. In addition, effects of process parameters on the wrinkling in the spinning process have been studied by the following researchers: Kleiner et al [2] concluded that in the conventional spinning the diameter and thickness of the workpiece had the most significant effects on the wrinkling failure. Hayama et al [5] reported that the feed ratio, sheet thickness and diameter were very important factors for the wrinkling in shear forming process. In general, if reducing the sheet thickness or increasing the feed ratio and sheet diameter the possibility of wrinkling failures will increase accordingly.

A concept of the geometric limit for wrinkling failure has been proposed in Tool and Manufacturing Engineers Handbook [6] to define the formability of a material in the metal spinning process. It is defined as the ratio of the cup depth (H) to the cup wall thickness (t). When a certain value of the cup depth to thickness ratio (H/t) is exceeded, wrinkles would occur. This limit value is related to a formability index which is defined as the ratio of the material's compressive modulus (E_c) and compressive yield stress (S_{cy}):

$$\text{Formability index} = \frac{E_c}{S_{cy}} \quad (1)$$

Although there is no detailed analysis offered in the aforementioned definitions, the relationship between the geometric limit and formability index is believed to be of practical value. Furthermore, by modifying the theory of the instability in the deep-drawing process, Kobayashi [7] proposed a theoretical model of flange wrinkling in conventional spinning. The instability in the flange of the conventional spinning would take place when

$$\frac{P_{\theta}}{E_p} \geq K \left(\frac{t}{w} \right)^2, \quad (2)$$

where P_{θ} is the mean tangential stress in the flange; E_p is the plastic buckling modulus; t is the current thickness of the flange; w is the current width of the flange and K is defined as a constant. Since this analytical model of flange wrinkling is adapted from deep drawing process, it may be only applicable for a single roller-pass process with linear roller path which traces along a cone shaped mandrel. However, in reality the conventional spinning is normally completed by multiple passes with non-linear roller path profiles. Therefore, although this work provides an insight into the theoretical analysis of the wrinkling failure, it does have its limitations.

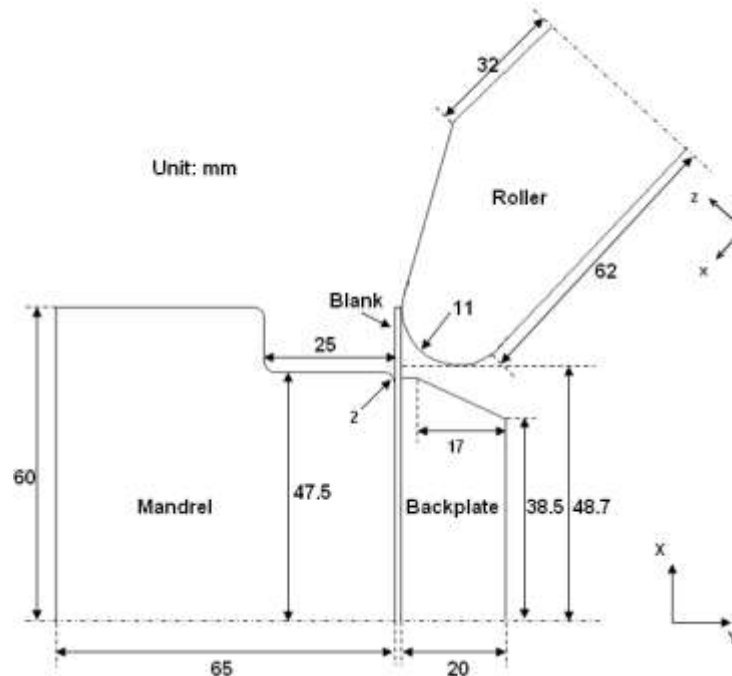
In this study, wrinkling failure of the spinning process has been investigated by both numerical and experimental methods. Based on a conventional spinning experiment, Finite Element models have been developed by using software Abaqus. FE models have been verified by studying the results obtained from models using different types of elements. Various energy histories are evaluated and the dimensions of the spun cylindrical cup obtained from the FE results are compared with the corresponding experimental results. Correlations have been found between FE analysis and experimental results. Based on the verified FE models, the severity of wrinkles has been quantified, variations of stresses and forces during the wrinkling, effects of the feed ratio on wrinkling failure as well as the wall thickness variation have been analysed. A formability diagram for wrinkling failure has been developed in relation to the roller feed ratio. Experimental results show that wrinkles can be smoothed out by a following roller pass, however high feed ratios will lead to rough surface finish of the spun part.

2. Experimental Investigation

An experiment has been carried out to study the wrinkling failures of conventional spinning process. Figure 3 shows the setup of this spinning experiment and its schematic diagram, where the angle between the roller axis and the mandrel axis is 45° . The metal sheet is made of mild steel (DC01). The thickness and original diameter of sheet is 1.2 mm and 120 mm , respectively.



a) Experimental setup



b) Schematic diagram and tool dimensions

Figure 3 Spinning experiment of wrinkling investigation

Figure 4 illustrates the roller passes used in the experiment, clearly only the two forward passes are effective as the backward pass does not deform the metal sheet. As shown in Figures 3 (b) and 4, axis-Y is defined as the axial direction of the mandrel and axis-X is the radial direction of the mandrel. Table 1 shows the process parameters used in four experimental runs. In an experimental run, the feed rate in the axial direction of the roller (z-axis in Figure 3b) is almost constant, while the feed rate in the radial direction of the roller (x-axis in Figure 3b) changes with time. 300% and 600% of the initial feed rate used in experimental run E1 are applied to

experimental run E2 and E3 respectively. Only the first pass of experimental run E3 is applied in experimental run E4.

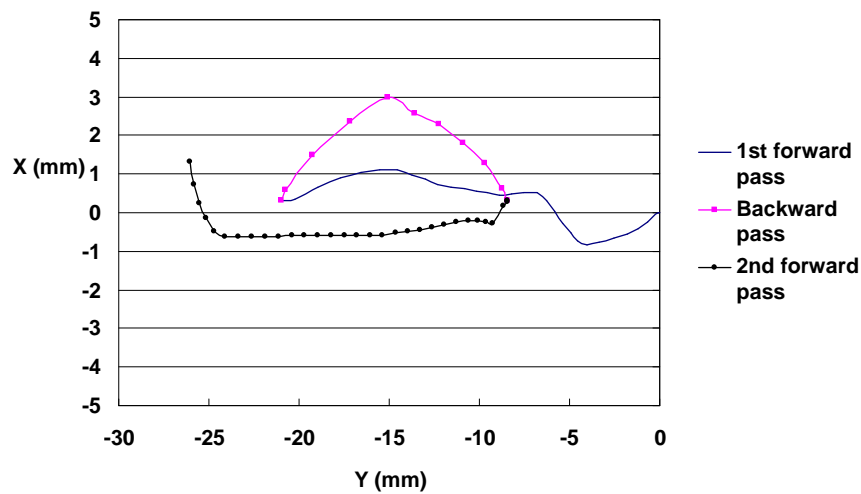


Figure 4 Roller passes used in the experiment

Table 1 Process parameters of experimental runs

Sample Number	Spindle Speed (<i>rpm</i>)	Longitudinal Feed Rate (<i>z</i> -axis) (<i>mm/min</i>)
E1	400	212 (Initial feed rate)
E2	400	300% * Initial feed rate
E3	400	600% * Initial feed rate
E4	400	600% * Initial feed rate (only the first roller pass is applied)

As shown in Figure 5(a), sample E1 has no wrinkles with relatively smooth surface. Increasing the initial feed rate by 300% and 600%, the surface of the sample E2 and E3 becomes rough accordingly, as shown in Figure 5(b) and 5(c). In addition, by comparing the experimental spun part E3 and E4 of Figure 5(c) and 5(d), it is clear that wrinkling occurs in the first forward pass, and then smoothed out during the second forward pass. However, the high feed rate of the roller pass leads to extremely rough surface finish, which also reported by Chen et al [8].

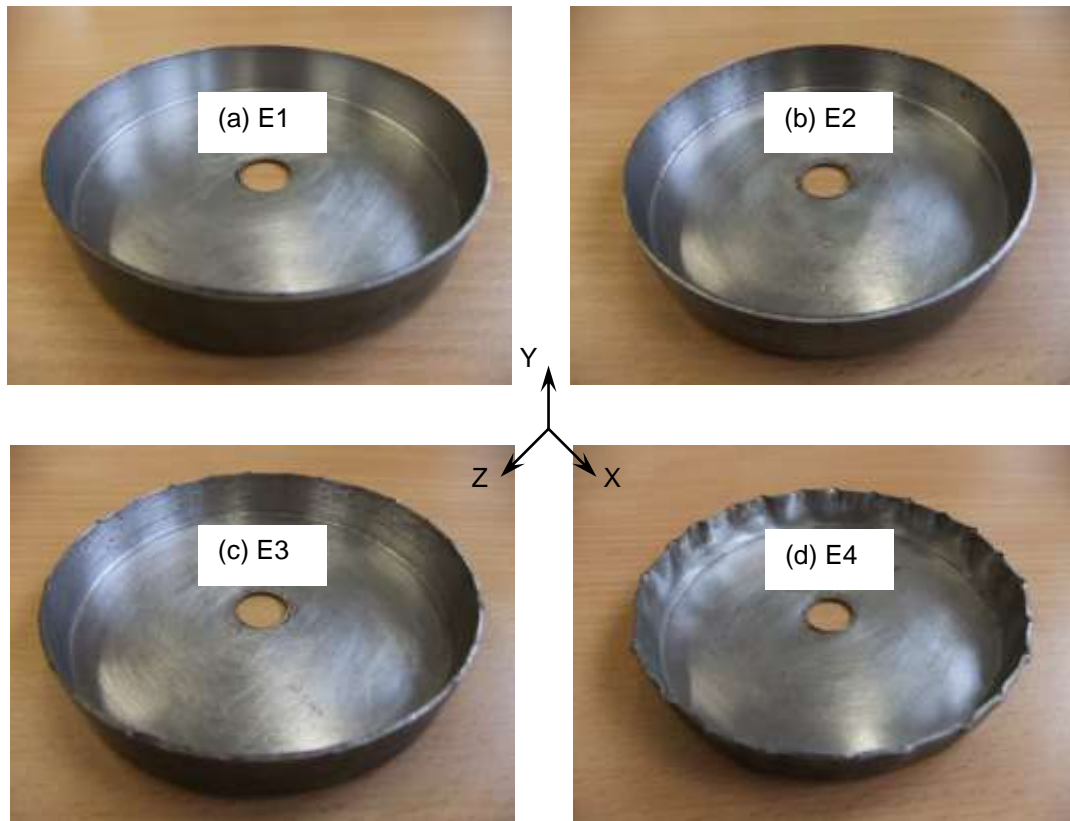


Figure 5 Experimental samples

3. Finite Element Analysis of Wrinkling

3.1 Solution Methods

Finite Element solution methods are generally resolved into implicit method and explicit method [9]. The implicit FE analysis method iterates to find the approximate static equilibrium at the end of each load increment. It controls the increment by a convergence criterion throughout the simulation. The implicit method is preferable to analyse some small 2-D problems and 3-D problems under simple loading conditions. On the other hand, the explicit FE analysis method determines a solution by advancing the kinematic state from one time increment to the next, without iteration. The explicit solution method uses a diagonal mass matrix to solve for the accelerations and there are no convergence checks. Therefore it is more robust and efficient for complicated problems, such as dynamic events, nonlinear behaviors, and complex contact conditions.

Metal spinning process can be considered as a quasi-static problem which includes large membrane deformation and complex contact conditions. Hence the explicit FE analysis method has been chosen to analyse the metal spinning process in this study. At the beginning of the increment (t), based on the dynamic equilibrium equation [10]:

$$P - I = M \ddot{u} \quad (3)$$

The nodal accelerations (\ddot{u}) are calculated as:

$$\ddot{u}|_{(t)} = (M)^{-1}(P - I)|_{(t)} \quad (4)$$

Where M is the nodal mass matrix, P is the vector of external applied force and I is the vector of internal element force. The acceleration of any node is completely determined by the mass and the net force acting on it. Through time the accelerations are integrated using the central difference rule, by which the change of the velocity is calculated from equation (5), assuming that the acceleration is constant:

$$\dot{u}|_{(t+\Delta t/2)} = \dot{u}|_{(t-\Delta t/2)} + \frac{\Delta t|_{(t+\Delta t)} + \Delta t|_{(t-\Delta t)}}{2} \ddot{u}|_{(t)} \quad (5)$$

The velocities are integrated through time and added to the displacement (u) at the beginning of the increment to calculate the displacements at the end of the increment:

$$u|_{(t+\Delta t)} = u|_{(t)} + \Delta t|_{(t+\Delta t)} \dot{u}|_{(t+\Delta t/2)} \quad (6)$$

In order to obtain accurate results from the explicit method, the time increment has to be extremely small which ensures that the acceleration through the increment is nearly constant. Therefore an explicit analysis typically require many thousands increments. The size of the increment is determined by the stability limit:

$$\Delta t = \min\left(\frac{L^e}{c^d}\right) \quad (7)$$

Where L^e is the characteristic element length, c^d is the wave speed of the material:

$$c^d = \sqrt{\frac{\lambda + 2\mu}{\rho}} \quad (8)$$

Where λ and μ are the Lamé's elastic constants, ρ is the material density. If T is the actual time of the analysed process, the number of the time increment required n can be obtained by:

$$n = \frac{T}{\Delta t} = \frac{T}{\min\left(L^e \times \sqrt{\frac{\rho}{\lambda + 2\mu}}\right)} \quad (9)$$

Normally it is unfeasible to run a quasi-static analysis with its real time scale, as the computing time may be extremely long. The mass scaling technique, which artificially increases the density of the material, is commonly used to speed up the analysis. According to equation (7) - (9), by increasing the mass density by a factor of f^2 , the number of the time increment will decrease by a factor of f . However, if a massive speed-up factor is applied, the corresponding inertial forces will affect the mechanical response and produce unrealistic dynamic results.

The general rule to control the inertial effects resulted from mass scaling is to ensure that the kinetic energy of the material should not exceed a small portion (typically 5%-10%) of its internal energy during the majority duration of the process [10].

3.2 Element Selection

The accuracy of any simulation highly depends on the type of element used in the simulation. Solid element and shell element are two of the most commonly used elements in metal forming simulation. During the metal spinning process the material undergoes a complicated loading process which includes bending effects [3-4]. Bending may cause “hourglassing” problem as a result of using reduced integration linear solid elements such as C3D8R in Abaqus, which could significantly affect the accuracy of simulation results [10]. As shown in Figure 6, the bending of a reduced integration linear solid element presents a zero-energy deformation mode, as no strain energy is generated by the element distortion [10]. Moreover, this “hourglassing” problem can propagate through the elements and produce meaningless numerical results.

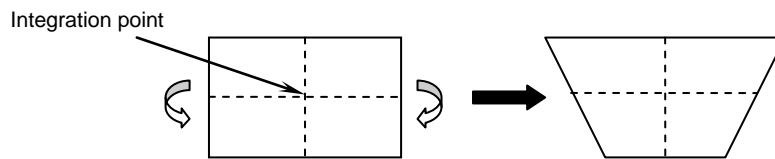


Figure 6 Deformation of a reduced integration linear solid element subjected to bending

On the other hand, unlike the reduced integration linear solid element, which only uses one integration point along the thickness direction, multiple integration points are used through the thickness of a shell element. Stresses and strains at each integration point of the shell element are calculated independently. 3-D 8 nodes reduced integration linear continuum shell element (SC8R in Abaqus) provides a better capability to model two-side contact behaviour and transverse shear deformation than 2-D conventional shell elements. Therefore it has been chosen to model the metal sheet in this study. In order to accurately compute the state of stresses through the sheet thickness, 9 integration points through the shell element thickness direction have been used, which is also suggested in [3] and [10]. Enhanced hourglass control, which provides an increased resistance to the hourglassing problem and more accurate displacement solutions than the default hourglass control [10], has been used in the FE analysis models. Detailed comparisons of the computational performance of the solid and shell elements used in the spinning simulation are given in Section 4.1.

3.3 Finite Element Modelling

In order to improve the computational efficiency, the spinning tools, i.e. the roller, mandrel and backplate are modelled as analytical rigid bodies, leaving the metal sheet as the only deformable body. The central area (radius of 30 mm) of the sheet is neglected, since it is clamped between the mandrel and the backplate and there is almost no material deformation taking place in this region. 5200 elements are used to model the metal sheet and the average aspect ratio of the mesh is about 1.3. The material of the metal sheet is assumed to be homogeneous and isotropic. The elastic behaviour of the material is defined by Young's modulus of 198.2 GPa, Poisson's ratio of 0.3, and mass density of 7861 kg/m³. The von Mises yielding criterion and isotropic hardening have been used to model the plastic response. The true stress-strain curve of mild steel, which is obtained from a tensile test, is shown in Figure 7. Strain rate and temperature effects are neglected in this study.

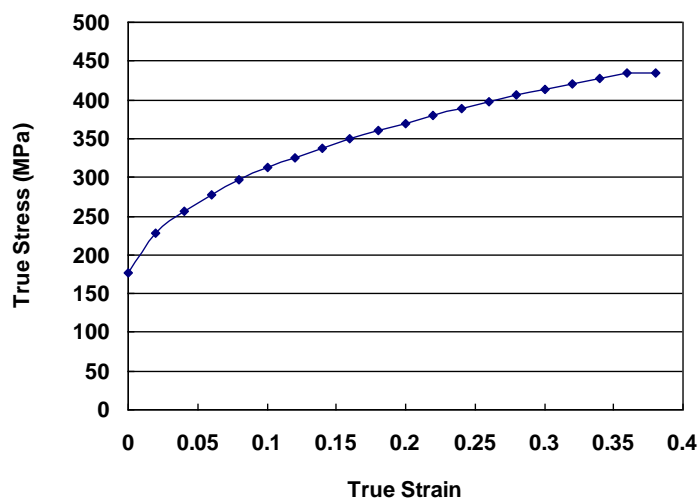


Figure 7 True stress-strain curve of mild steel (DC01)

The penalty constraint enforcement method has been used to simulate the contact between the metal sheet and tools. It has been shown to provide good results in the spinning simulations [11-13]. Coulomb's friction law is used to model the interface behaviour between the tools and sheet. As the roller rotates along its own axis during the spinning process, the frictional coefficient between the roller and the sheet is artificially set to be low. Three Coulomb's frictional coefficients have been assigned to three contact pairs of the tooling and sheet: roller-sheet 0.02, mandrel-sheet 0.2, backplate-sheet 0.5. Three analysis steps have been used in the spinning simulation [14]: at the beginning of the spinning simulation, a compressive force of 20 kN is applied on the backplate, which makes the sheet to be clamped between the backplate and the mandrel. A rotational boundary condition is applied on the backplate and the mandrel, resulting in the sheet, backplate and mandrel to rotate synchronously at a specified spindle speed. Displacement boundary conditions, which are calculated from the

recorded CNC program of the experiment, are applied on the roller to perform the complex non-linear roller passes.

Since the wrinkling failures only take place in the first forward roller pass of the experiment, the second forward pass is neglected in the FE models. Table 2 presents the process parameters of some of the FE models and the corresponding flange states. The mass scaling technique is used in these FE models to speed up the computation. A mass scaling factor of 25 has been used in Model 1 - 6, in which the spindle speed varies between 400 *rpm* to 800 *rpm*. Conversely, no mass scaling is used in Model 7, which applies a significantly high spindle speed – 1800 *rpm*, in order to prevent the inertial effects due to mass scaling, as discussed in section 4.3. The feed ratio is defined as the ratio of feed rate to the spindle speed. The first three models (Model 1 - Model 3) use the same experimental setting as experimental sample E1, E2 and E4.

Table 2 FE analysis process parameters and flange state of spun part

Model	Replay feed rate	Feed rate (mm/min)	Spindle speed (rpm)	Mass scaling factor	Feed ratio (mm/r)	Process duration (s)	Flange state
Model 1	100%	212	400	25	0.53	5.44	No wrinkles
Model 2	300%	636	400	25	1.59	1.81	Wrinkling
Model 3	600%	1272	400	25	3.18	0.91	Wrinkling
Model 4	800%	1696	800	25	2.12	0.68	Wrinkling
Model 5	200%	424	600	25	0.71	2.72	No wrinkles
Model 6	600%	1272	800	25	1.59	0.91	Wrinkling
Model 7	600%	1272	1800	1	0.71	0.91	No wrinkles

4. Verification of FE Models

4.1 Element Selection

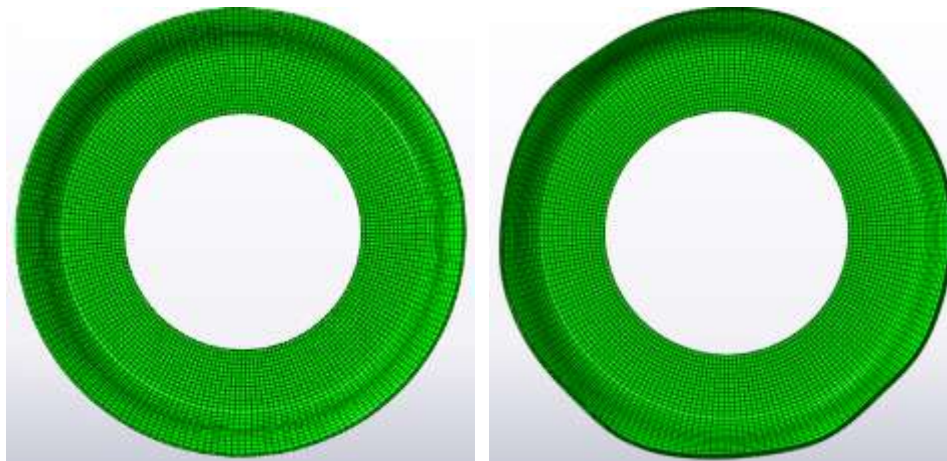
To evaluate the performance of 8 nodes reduced integration linear solid element (C3D8R) and 8 nodes reduced integration linear continuum shell element (SC8R) for the wrinkling simulation of spinning process, three FE models have been compared using the experimental setting of sample E4. Detailed meshing information is shown in Table 3, where Model 3a and 3b applied the same process parameters as Model 3 defined in Table 2, but with different element types and the number of elements through thickness direction of the metal sheet.

Table 3 FE models using different types and numbers of elements

Model		Type of element	Number of elements through thickness	Number of element	Stable increment (s)	Computation time (hour:min:sec)	Flange state
Wrinkling Model	Model 3a	C3D8R	1	5200	4.71e-7	08:51:12	No wrinkles
	Model 3b	C3D8R	4	20800 (5200*4)	1.37e-7	48:09:38	Minor wrinkles
	Model 3	SC8R	1	5200	5.66e-7	14:18:07	Severe wrinkles
Wrinkle-free Model	Model 5a	C3D8R	1	5200	5.12e-7	13:14:48	No wrinkles
	Model 5b	C3D8R	4	20800 (5200*4)	2.12e-7	62:55:34	No wrinkles
	Model 5	SC8R	1	5200	5.66e-7	21:44:38	No wrinkles

* Mass scaling factor 25

Figure 8 compares the deformed workpieces of these FE models with the corresponding experimental sample. As shown in Figure 8(a), although extremely fine mesh has been used, Model 3a, which uses one single layer of solid elements in the thickness direction, cannot capture the wrinkling failure occurred in the experiment. Using four layers of elements through the thickness direction slightly improves the results, where minor wrinkling is observed on the deformed FE workpiece, as shown in Figure 8(b). However, it is still unable to represent the real severe wrinkles of the experiment sample as shown in Figure 8(d). On the other hand, Model 3, which uses a single layer of continuum shell elements in the thickness direction, produces much better results, as shown in Figure 8(c). By increasing the number of the solid element layers through the thickness direction could improve FE results, but it is computational unfeasible to carry out a spinning process simulation using a FE model with several element layers in the thickness direction. Extremely long computing time is required not only due to an extremely fine mesh but also an extremely small element length which significantly decreases the stability limit value of the explicit solution, according to equation (7). In this study, it has shown that the computing time of Model 3b is almost four times of that of Model 3, as details given in Table 3.



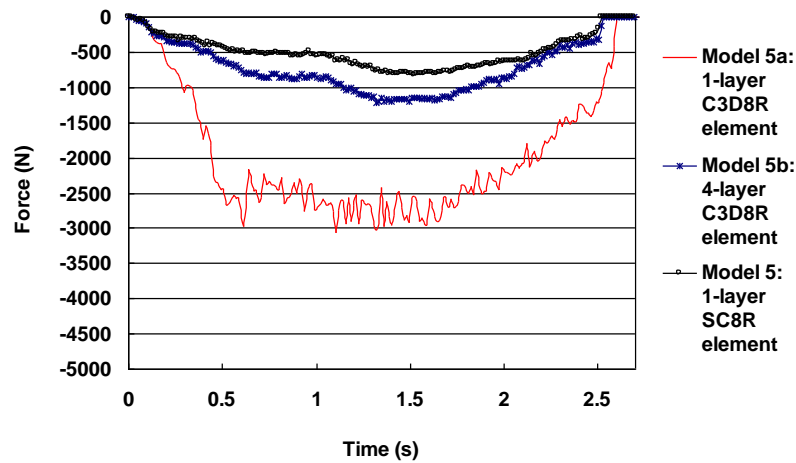
(a) Model 3a (1-layer of solid element) (b) Model 3b (4-layers of solid element)



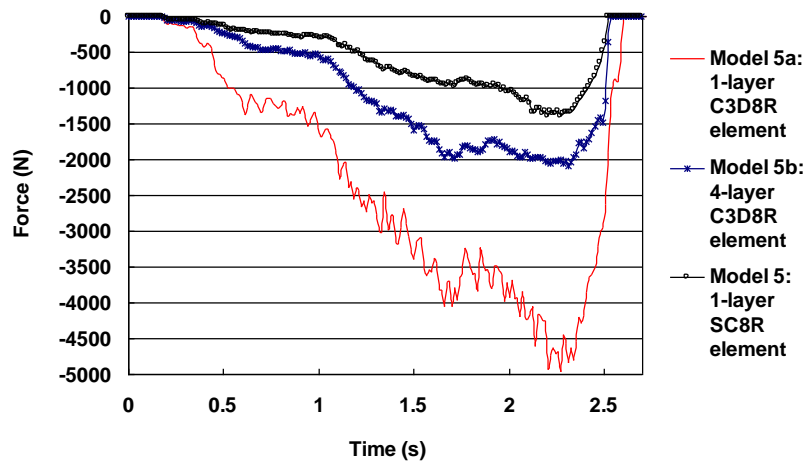
(c) Model 3 (1-layer of continuum shell element) (d) Experimental sample (E4)

Figure 8 Comparison of deformed workpiece using different types and numbers of elements

To further investigate the effects of the two element types on spinning simulation not involving wrinkling, force simulation results along the axial and radial directions of the mandrel obtained from wrinkle-free models – Model 5a, 5b and 5 have been analysed. As can be seen from Figure 9, the tool forces of Model 5a, which uses one layer solid elements in thickness, are about three times higher than the corresponding values of Model 5 where one layer of continuum shell elements in thickness is used. By using four layers of the solid element in Model 5b, the force values are significantly decreased, as a result of using four integration points through the thickness direction. However, the forces are still higher than the corresponding values obtained from Model 5 that uses one layer continuum shell elements, where the maximum difference is approximately 50%. The overestimation of the tool forces by Model 5a and 5b may be resulted from the artificially introduced high hourglass control stiffness which is adapted in Abaqus in order to limit the propagation of “hourglassing” deformation mode.



(a) Axial forces



(b) Radial forces

Figure 9 Force comparisons of wrinkle-free models using different types and numbers of elements

Based on the above analysis, the reduced integration linear solid element is unable to accurately represent the wrinkling failure in the spinning process. In addition, these two types of element produce very different values of forces when modelling the wrinkle-free models. This may be caused by the “hourglassing” problems which the reduced integration linear solid elements suffer from, as further discussed in Section 4.3 of the energy distribution study. The preliminary findings suggest that the reduced integration linear solid element is not suitable for the metal spinning simulation. This may be agreed with Tekkaya [15], who suggested that solid elements were seldom used for the simulation of sheet metal forming.

4.2 Dimensions of Spun Cylindrical Cup

The number of wrinkles, the height and thickness variations of the experimental spun cup have been measured to verify the FE models. By comparing Figure 8(c) and Figure 8(d), there are 20 wrinkles according to the FE

results of Model 3, whereas 24 wrinkles are observed in the experimental sample E4. The difference may be resulted from that some of the minor wrinkles on the experimental sample are difficult to be captured in the FE model. The average height of the FE sample is about 13.8 mm, while approximately 14 mm has been measured from the experimental sample. Figure 10 compares the thickness distributions of a cross section of the spun cup using FE analysis Model 3 and the corresponding experimental sample E4, where 4% error bars are used. The maximum error of wall thickness results between the experiment and FE simulation is 5.11%. Considering that the wrinkles have been generated on the spun part and the thickness of the part is very small (1.2 mm), a maximum error of 5.11% in thickness (0.06 mm) demonstrates the correlation between the experiment and FE simulation.

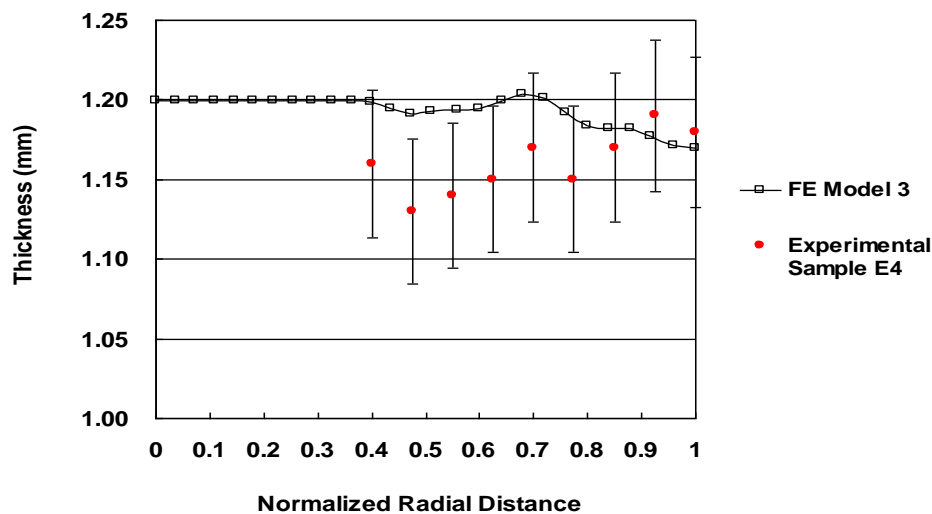


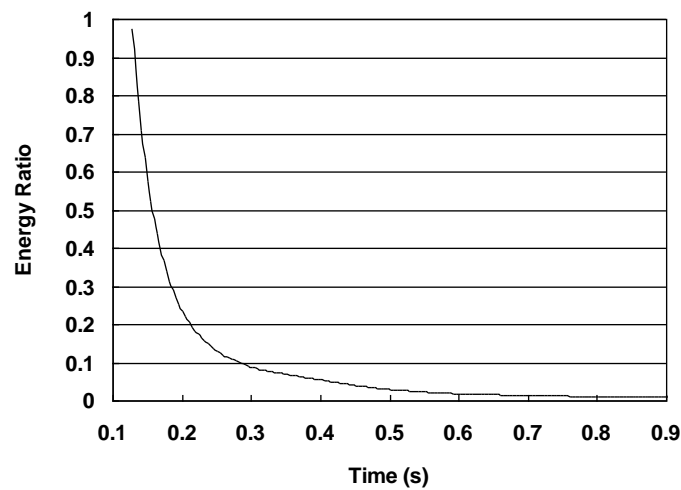
Figure 10 Comparison of wall thickness between FEA and experimental results

4.3 Energy Distribution

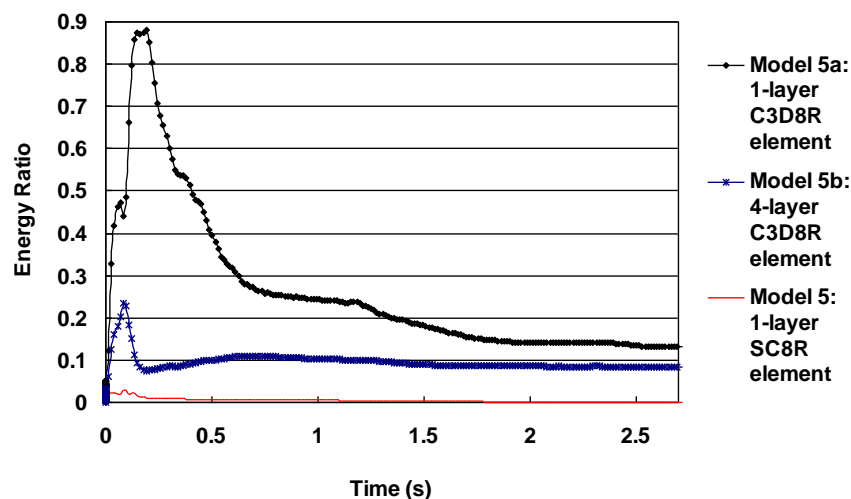
Various energy distributions of the FEA model have also been analysed to evaluate the simulation results. Two criteria are used in this study, as also suggested in [10]. In order to ensure that the inertial effects due to mass scaling do not significantly affect the simulation results, the kinetic energy of the workpiece should be no greater than 10% of its internal energy during the majority duration of the spinning process. In addition, the ratio of artificial strain energy, which is caused by artificial hourglass control of the reduced integration linear elements, to the internal energy should be less than 5%, so that the “hourglassing” does not affect the FE analysis results.

Figure 11(a) shows the ratio of the kinetic energy to the internal energy of the workpiece in the wrinkling model – Model 3. Clearly, the energy ratio is extremely high at the beginning of the spinning process, because at this stage the rotation of the workpiece dominates while only small plastic deformation takes place. As the spinning progresses, the plastic deformation increases significantly, resulting in a sharply decreasing of the ratio. The ratio of the kinetic energy to the internal energy is below 10% during two thirds of the process, indicating that the solution is quasi-static and thus the inertial effects due to mass scaling is well controlled.

Figure 11(b) compares the ratios of the artificial strain energies to the internal energies from the three wrinkle-free models – Model 5a, 5b and 5. It is clear that the energy ratio is around 1% throughout the whole process in Model 5 which uses one layer continuum shell elements, demonstrating that “hourglassing” is not an issue in this model. However, the energy ratio is extremely high in Model 5a with one layer of solid elements. It shows that “hourglassing” is a major problem which could significantly affects the results. By using 4 layers of solid elements in Model 5b, this energy ratio has decreased dramatically but is still much higher than the energy ratio obtained from Model 5. It is believed that the “hourglassing” problem suffered by the reduced integration linear solid element is the reason that it cannot represent wrinkling failures and delivery accurate force results in the spinning FE simulation.



a) Ratio of kinetic energy to internal energy of the wrinkling model – Model 3



b) Ratio of artificial strain energy to internal energy of the wrinkle-free models – Model 5a, 5b and 5

Figure 11 Distributions of kinetic, internal and artificial strain energy

5. Results and Discussion

5.1 Severity of Wrinkles

Deformed workpieces obtained from Model 2, 4 and 5 defined in Table 2 are shown in Figure 12, which suggests that with an increasing feed ratio, wrinkling failure tends to take place. Moreover, the severity of wrinkles increases accordingly when applying higher feed ratios. In order to quantify the severity of wrinkles, the radial fluctuation of the cup flange edge from the nominal position of the roller path is expressed by radial coordinates of the element nodes located on the edge of the deformed workpiece along the circumferential direction. These are plotted in Figure 13.



(a) Model 5 (0.71 mm/rev) (b) Model 2 (1.59 mm/rev) (c) Model 4 (2.12 mm/rev)

Figure 12 Effects of roller feed ratio on wrinkling

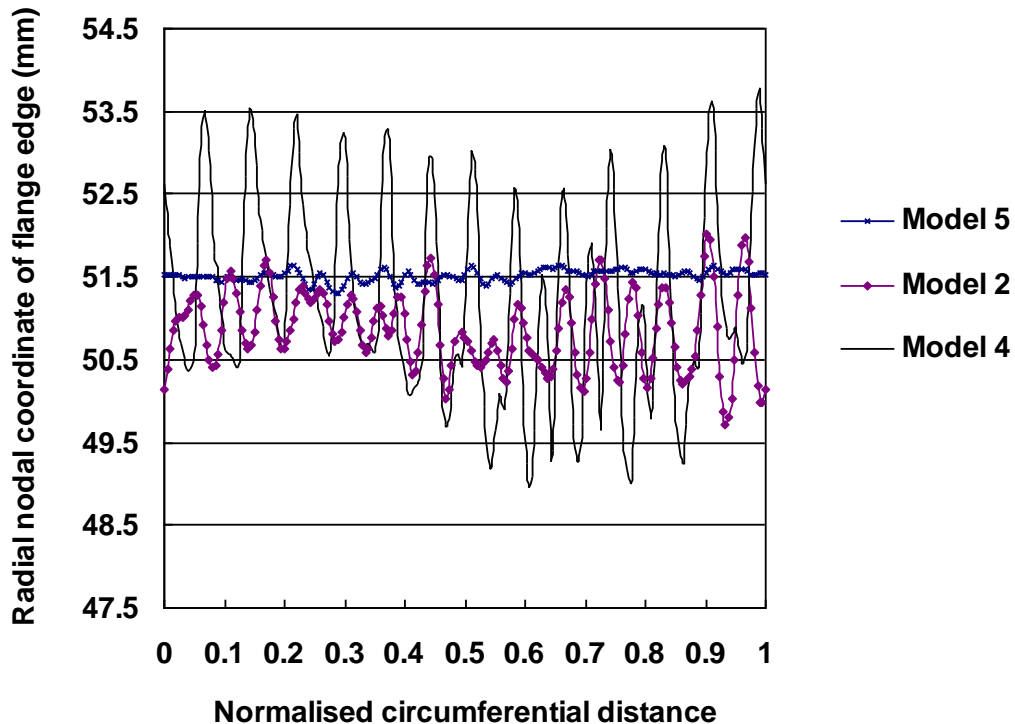


Figure 13 Severity of wrinkles of FE models

The mean, maximum, minimum and standard deviations of these radial coordinate values, which illustrate various degrees of the wrinkles, are calculated by equation (10) and (11) and shown in Table 4.

$$\bar{U} = \frac{\sum_{i=1}^N U_i}{N} \quad (10)$$

$$s = \sqrt{\frac{1}{N-1} \sum_{i=1}^N (U_i - \bar{U})^2} \quad (11)$$

Where \bar{U} is the mean value of these radial coordinate, U_i is the radial coordinate of node i and N is the number of the nodes along the edge of flange in the FE model.

Table 4 Standard deviations of wrinkle amplitudes

Model	Feed ratio (mm/rev)	Maximum radial coordinate (mm)	Minimum radial coordinate (mm)	Mean radial coordinate (mm)	Standard deviation (mm)
Model 5	0.71	51.645	51.304	51.515	0.068
Model 2	1.59	52.020	49.721	50.842	0.467
Model 4	2.12	53.791	48.965	51.132	1.179

As shown in Table 4, it is clear that when the feed ratio is 0.71 mm/rev, the standard deviation of the radial coordinates of the element nodes on the edge of the deformed workpiece is 0.068 mm, indicating no wrinkling takes place in Model 5, as shown in Figure 12. However, by increasing the feed ratios to 1.59 mm/rev and 2.12 mm/rev, the standard deviation of the radial coordinates increase to 0.467 mm and 1.179 mm, respectively. It confirms that the severity of the wrinkles increases exponentially when increasing the feed ratio.

5.2 Forming Limit of Wrinkling

A formability study has been carried out by applying different combinations of the feed rate and spindle speed in the FE models. A feed ratio of 0.71 mm/r has been found to be the forming limit of wrinkling for the spinning process considered, beyond which wrinkling failures will take place. A forming limit diagram for wrinkling is illustrated in Figure 14, which also confirms that the wrinkling tends to occur when using high feed rates or low spindle speeds. In other word, using high feed ratio increases the possibility of the wrinkling failure. This finding has also been confirmed in the experimental investigations of both shear forming [5] and one-pass deep drawing spinning [16]. The wrinkling zone and wrinkling-free zone is approximately separated by a straight line,

as shown in Figure 14. It suggests that as long as keeping the feed ratio below the feed ratio limit, increasing the feed rate and spindle speed proportionally, the wrinkle failure can be prevented, as also reported in [5].

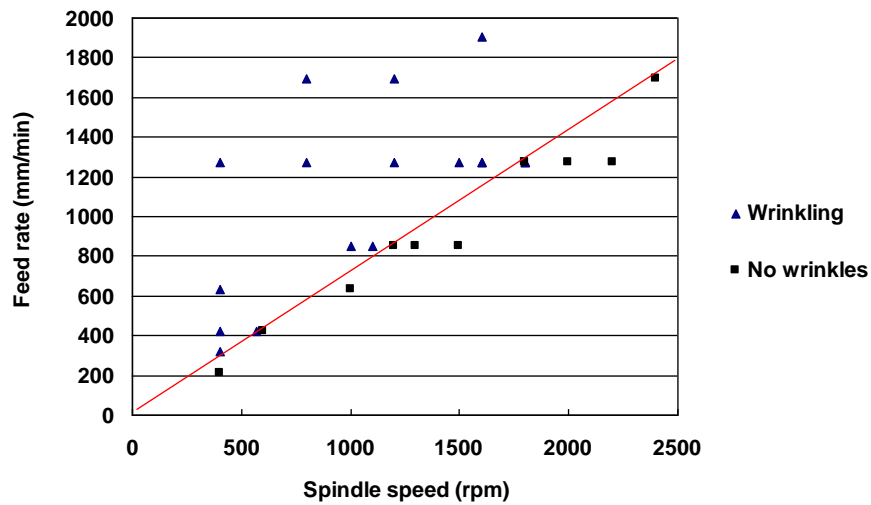


Figure 14 Forming limit diagram for wrinkling

However, the feed ratio limit obtained in Figure 14 is only valid for this specific experimental setting. The feed ratio limit depends on a number of key parameters of the spinning process, such as the sheet material, sheet thickness, sheet diameter and roller path etc. In this paper, the effects of sheet thickness have also been investigated. As shown in Table 5, the feed ratio limit increases when using thicker metal sheets. It suggests that the thicker the metal sheet, the higher capability to stand the wrinkling failure, as also claimed by Kleiner et al [2] and Xia et al [16].

Table 5 Feed ratio limits of various thicknesses of metal sheets

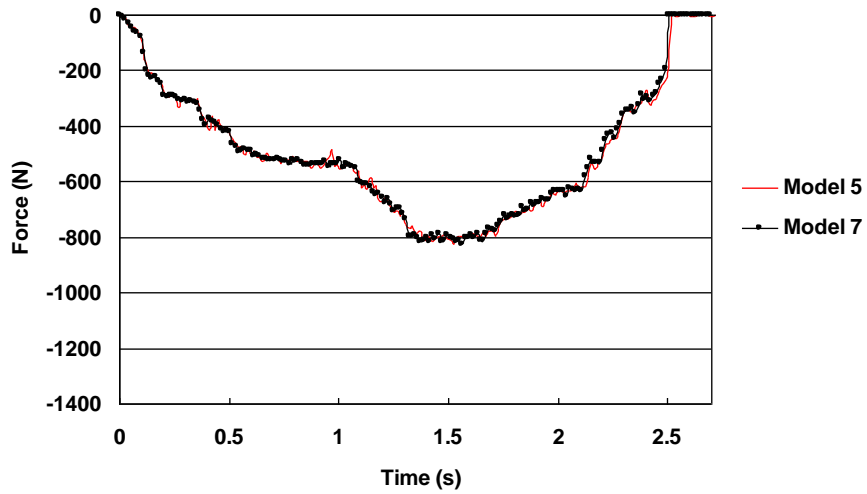
Thickness of sheet (mm)	Feed ratio limit of wrinkling (mm/rev)
1.2	0.71
1.6	1.06
2.0	1.88

5.3 Tool Forces

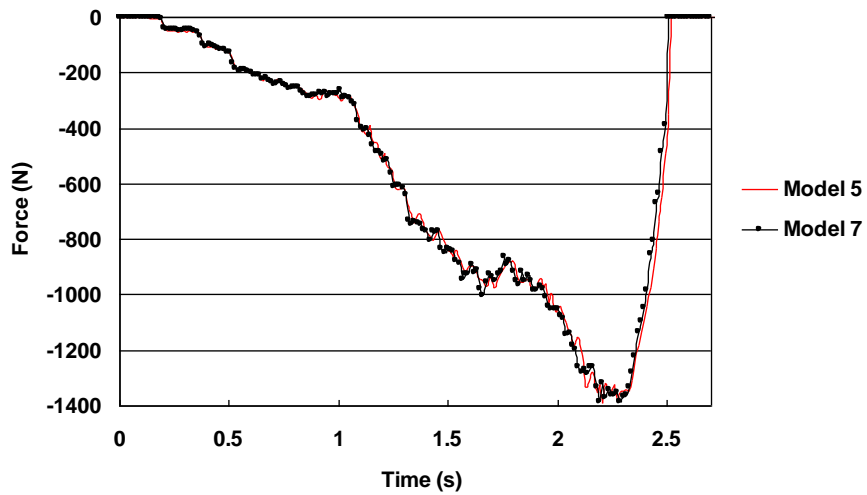
In this study, the total tool force of the spinning process has been resolved into three perpendicular components: the axial force is defined as the force in line with axis of the mandrel; the radial force is defined as the force parallel to the radial direction of the mandrel; and the tangential force is perpendicular to both the axial and radial tool forces. Figure 15 compares the tool force components of the two wrinkle-free models - Model 5 and Model 7 as defined in Table 2, which use the same feed ratio but with different spindle speeds and feed rates. Clearly, the corresponding tool force components are almost exactly the same. This supports the assertion that

as long as keeping the feed ratio constant, by changing the feed rate and the spindle speed proportionally, there would be no significant effects on the final spun product. Furthermore, during the spinning process the tangential force is the smallest among three force components, which has been also reported in published papers for both conventional spinning [16 and 17] and shear forming [18 and 19]. In the initial stage of the spinning, because the workpiece is mainly subjected to bending effects [4, 20-22], the axial force is greater than the radial force. At the middle stage of the process, the axial force begins to decrease due to the remaining flange decreases gradually; while the radial force continues to increase and peaks at the end of the process. This may be a result of the roller forcing the sheet towards the mandrel at the final stage, as corresponding to the roller passes shown in Figure 4.

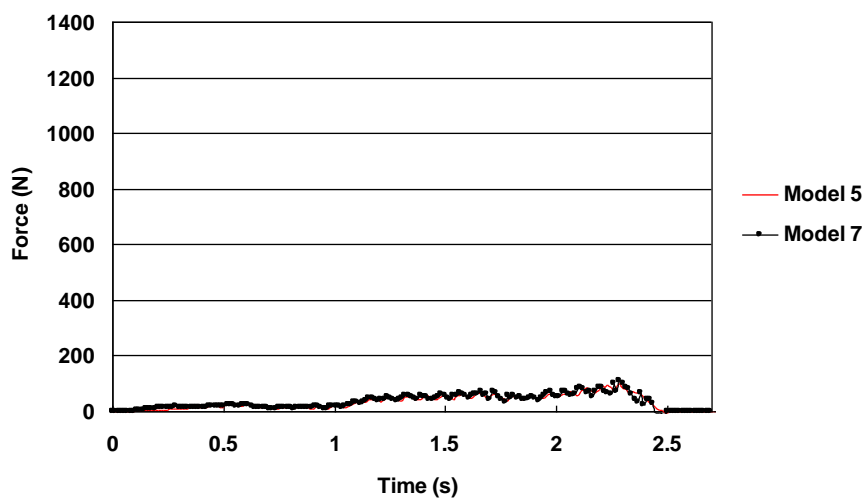
Figure 16 illustrates the force history of wrinkling model – Model 4. Comparing with the corresponding forces of wrinkle-free model shown in Figure 15, the magnitudes of the forces are much higher at the second half stage of the spinning process, when severe deformation takes place due to wrinkles appearing on the flange. In addition, according to Figure 16, sudden changes and fluctuations of forces are clearly shown from 0.34 s onwards. These sudden changes and fluctuations of tool forces may be resulted from the existing wrinkles on the workpiece interacting with the roller. As shown in Figure 17, wrinkling failure initiates at 0.34 s and is extending to the whole flange around 0.36 s. Consequently it is considered that these sudden changes and fluctuations in tool forces may be used to determine the moment when wrinkling occurs, as also reported by Kleiner et al [2], Arai [18], Hayama [19], Finckenstein and Dierig [23].



(a) Axial force

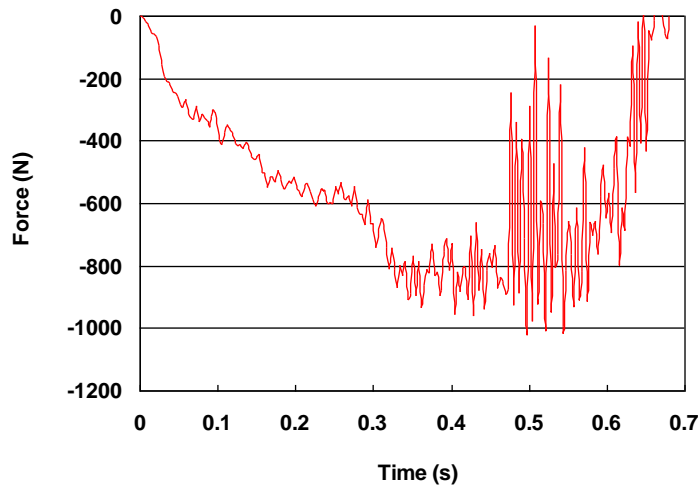


(b) Radial force

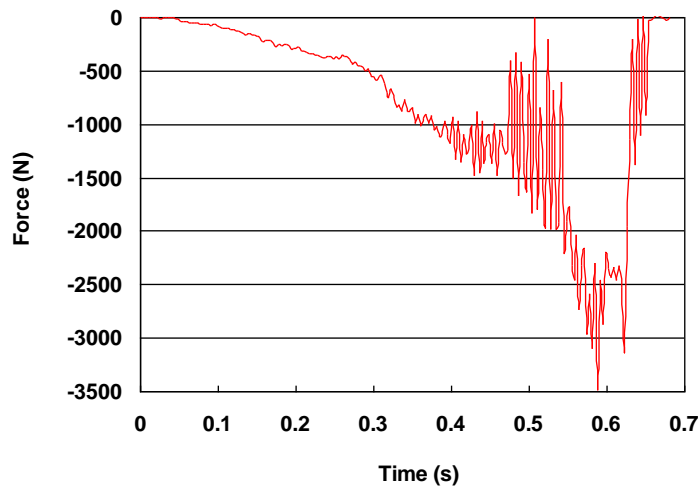


(c) Tangential force

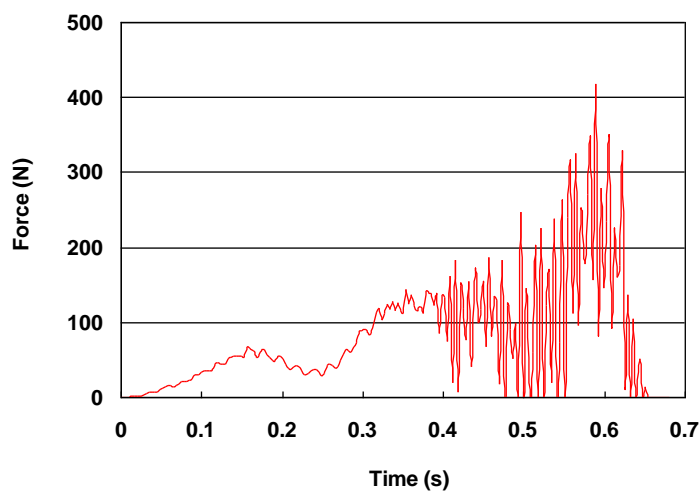
Figure 15 Force histories of wrinkle-free models (Model 5 and 7)



(a) Axial force



(b) Radial force



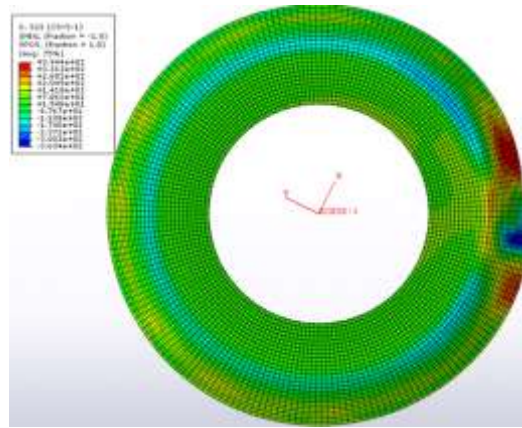
(c) Tangential force

Figure 16 Force histories of wrinkling model (Model 4)

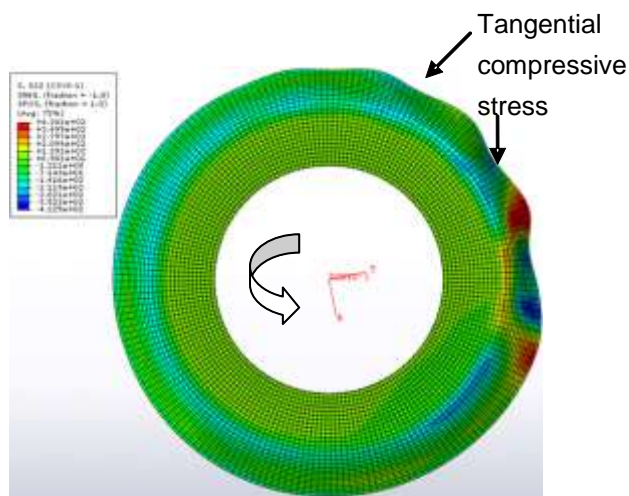
5.4 Stresses

By comparing variations of the axial and radial stress distributions in the wrinkling model (Model 4) with that of the wrinkle-free model (Model 5), there is a distinct difference between the tangential stress distributions of these two models. Figure 17 shows the tangential stress distributions through the wrinkling developing process in Model 4. Figure 18 shows the tangential stress distributions of the wrinkle-free model – Model 5 at the corresponding stages. According to Figure 17(a) and 18(a), at Stage 1 there is no apparent difference of the tangential stress distributions between these two models. As can be seen from Figure 17(b), wrinkles take place around processing time of 0.34 s. The compressive tangential stresses distribute not only in the roller contact zone but also in other areas of the flange. At stage 3 shown in Figure 17(c), the compressive tangential stresses locate regularly along the circumferential direction of workpiece and more wrinkles are generated. Conversely, at the corresponding stages of the wrinkling-free model illustrated in Figure 18(b) and 18(c), there are no compressive tangential stresses observed on the flange area, except for at the roller contact zone.

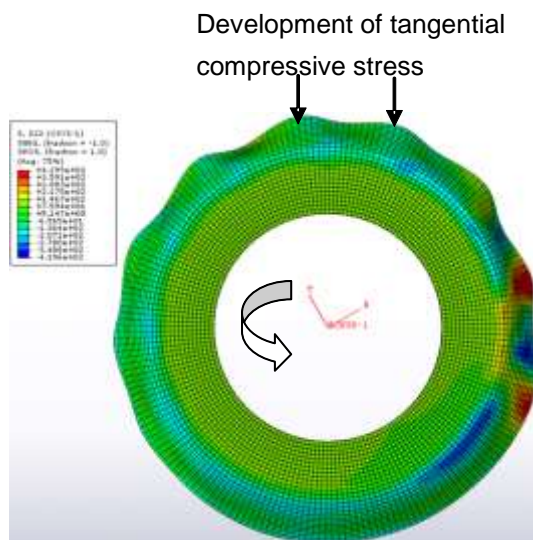
It is believed that in the wrinkle-free model, the compressive tangential stresses “recover” to tensile tangential stresses when the current contact area moves away from the roller. Conversely, in the wrinkling model the compressive tangential stresses induced at the roller contact zone do not fully “recover” to tensile tangential stresses after being deformed. This may be because that the compressive stresses at the roller contact zone are beyond the buckling stability limit, resulting in some compressive tangential stresses remains in the previous contact zone thus leading to the wrinkling failure. Runge [1] and Köhne [24] also believed that the tangential stress was responsible for the wrinkling failure in the spinning process.



(a) Stage 1, time = 0.295 s

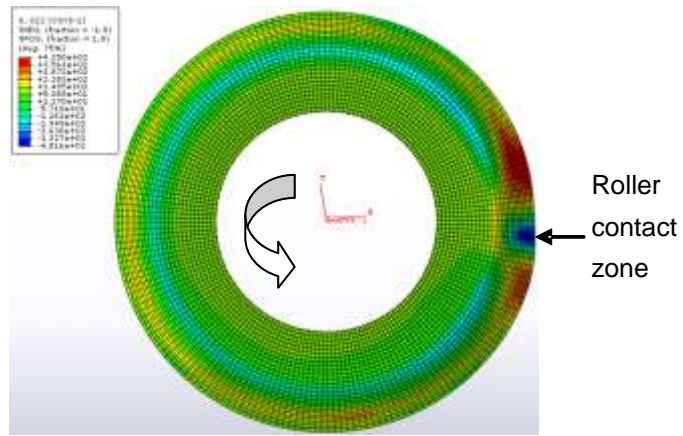


(b) Stage 2, time = 0.34s

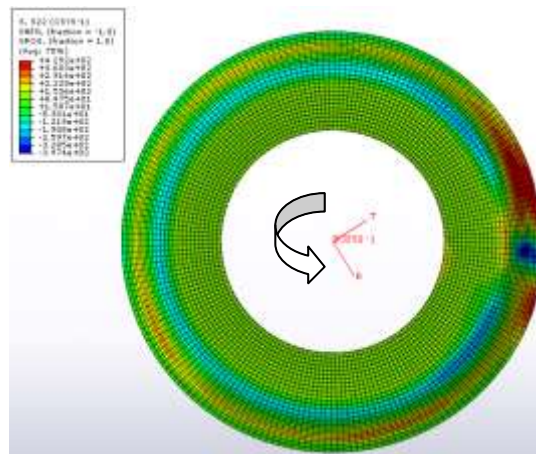


(c) Stage 3, time = 0.363s

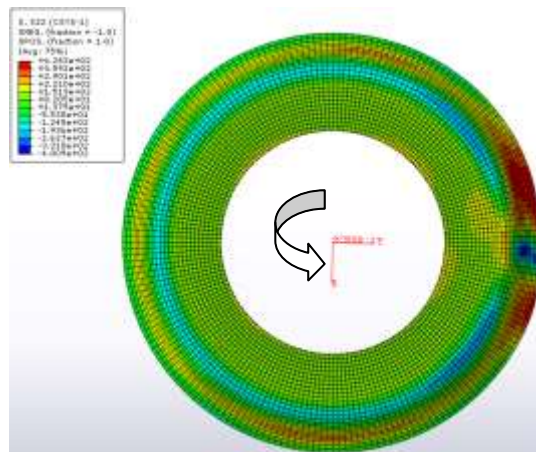
Figure 17 Tangential stress distribution of wrinkling model (Model 4)



(a) Stage 1, time = 1.179s



(b) Stage 2, time = 1.360s



(c) Stage 3, time = 1.451s

Figure 18 Tangential stress distribution of wrinkle-free model (Model 5)

5.5 Thickness

Figure 19 illustrates the effects of feed ratio on the wall thickness distribution of the spun cylindrical cup. Clearly, less thinning of the wall thickness takes place if high feed ratio is applied. This finding agrees with Runge [1] who suggests that lower feed ratios produce excessive material flow to the edge of the workpiece and unduly thin the wall thickness. Material shearing between the roller and workpiece due to frictional effects may be the main reason of the sheet thinning. Considering the roller feeding the same distance during the spinning process, when using a lower feed ratio, the roller will scan the workpiece with more revolutions, thus leading to higher shearing effects than spinning at a high feed ratio. It is clear that in order to maintain the original sheet thickness unchanged, high feed ratios should be used. However, high feed ratios could lead to rough surface finish and material failures, as discussed in Section 2 and Section 5.1. Therefore it is necessary to find a “trade-off” feed ratio, which not only can help to maintain the original sheet thickness unchanged but also prevent the material failures and produce good surface finish.

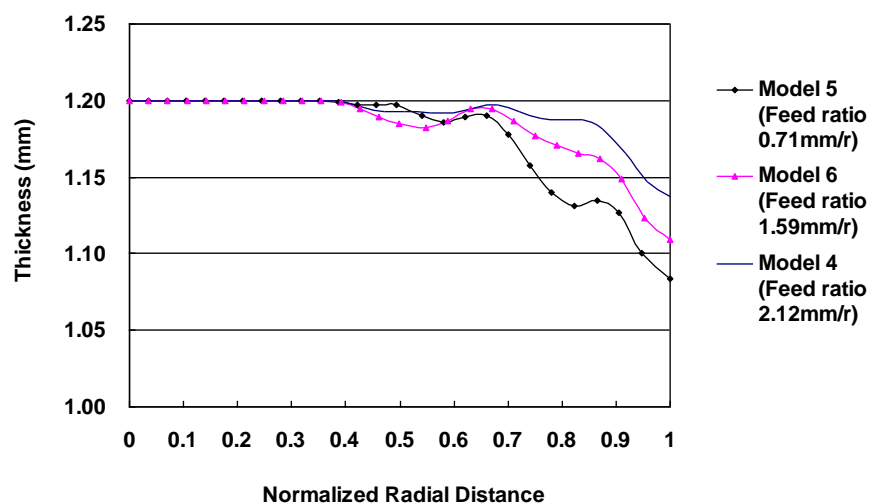


Figure 19 Wall thickness distributions at different feed ratios

6. Conclusions

- This study has shown that the reduced integration linear solid element is not suitable for the metal spinning simulation, due to the “hourglassing” problem it suffered from. And the reduced integration linear continuum shell element is ideal to simulate the spinning process.
- The severity of the wrinkles is quantified by calculating the standard deviation of the radial coordinates of element nodes on the edge of the flange of the spun cup in the FE models. The results have shown that the severity of the wrinkles increases exponentially when increasing the feed ratio.

- c) A forming limit study of wrinkling indicates that there is a feed ratio limit beyond which wrinkling failures will occur. Provided keeping the feed ratio below the limit, by increasing the feed rate and spindle speed proportionally, wrinkling failures can be prevented.
- d) Compressive tangential stresses have been observed at the flange area near the local forming area but these will change into tensile tangential stresses when the sheet rotates away from the current roller contact zone. However, if the compressive tangential stresses do not fully “recover” to tensile tangential stresses after roller contact, wrinkling failure may take place.
- e) Sudden changes and fluctuations of the tool forces, resulted from existing wrinkles on the workpiece interacting with the roller, could be used to determine the approximate moment of wrinkling occurrence.
- f) High feed ratios help to maintain the original sheet thickness unchanged. However, high feed ratios also lead to wrinkling failures and rough surface finish. It is necessary to find a “trade-off” feed ratio in the spinning process design.

Acknowledgements

The authors would like to acknowledge the financial support from the UK Technology Strategy Board (TSB) and Metal Spinners Group Limited, Project No. 6590.

Reference

- [1] **Runge, M.** Spinning and Flow Forming, (D. H. Pollitt, Trans), Leifield GmbH, 1994;
- [2] **Kleiner, M., Gobel, R., Kantz, H., Klimmek, Ch., and Homberg, W.** Combined Methods for Prediction of Dynamic Instabilities in Sheet Metal Spinning, *CRIP Annals-Manufacturing Technology*, 2002, **51(1)**, 209-214;
- [3] **Klimmek, Ch., Gobel, R., Homberg, W., Kantz, H., and Kleiner, M.** Finite Element Analysis of Sheet Metal Forming by Spinning, *Advanced Technology of Plasticity, Vol2, Proceedings of 7th ICTP*, Yokohama, Japan Oct. 28-31, 2002;
- [4] **Sebastiani, G., Brosius, A., Homberg W., and Kleiner, M.** Process Characterization of Sheet Metal Spinning by Means of Finite Elements, *Key Engineering Materials*, 2007, **334**, 637-644;
- [5] **Hayama, M., Murota, T., and Kudo,, H.** Deformation Modes and Wrinkling of Flange on Shear Spinning, *Bulletin of JSME*, 1966, **9(34)**, 423-433;
- [6] **Wick, C., Benedict, J. T., and Veilleux, R. F.** Tool and Manufacturing Engineers Handbook, Volume 2 – Forming, 4th Edition, Society of Manufacturing Engineers, 1984, USA;

- [7] **Kobayashi, S.** Instability in Conventional Spinning of Cones, *Journal of Engineering for Industry-transactions of the ASME*, 1963, **85** (series B), 44-48;
- [8] **Chen, M. D., Hsu, R. Q., and Fuh, K. H.** Forecast of Shear Spinning Force and Surface Roughness of Spun Cones by Employing Regression Analysis, *International Journal of Machine Tools and Manufacture*, 2001, **41**, 1721-1734;
- [9] **Harewood, F. J. and McHugh, P. E.** Comparison of Implicit and Explicit Finite Element Methods Using Crystal Plasticity, *Computational Material Science*, 2007, **39**, 481-494;
- [10] Abaqus Analysis User's Manual, Abaqus. Inc., Version. 6.8, 2008;
- [11] **Bai, Q., Yang, H., and Zhan, M.** Finite Element Modelling of Power Spinning of Thin Walled Shell with Hoop Inner Rib, *Transactions of Nonferrous Metals Society of China*, 2008, **18**, 6-13;
- [12] **Liu, C.** The Simulation of the Multi-Pass and Die-Less Spinning Process, *Journal of Materials Processing Technology*, 2007, **192-193**, 518-524;
- [13] **Zhao, J., Champlaud, H., and Dao, T.** Simulation of Shear Spinning Process Using Finite Element Method, *Proceedings of the 18th IASTED International Conference Modelling and Simulation*, Montreal, Quebec, Canada, May 30-June 1, 2007, , pp. 239-245;
- [14] **Hamilton, S. and Long, H.** Analysis of Conventional Spinning Process of a Cylindrical Part using Finite Element Method, *Special Edition of Steel Research International*, Verlag Stahleisen GmbH, 2008, **79(1)**, 632-639;
- [15] **Tekkaya, A.** State-of-the-art of Simulation of Sheet Metal Forming, *Journal of Materials Processing Technology*, 2000, **103** , 14-22;
- [16] **Xia, Q., Shima, S., Kotera, H., and Yasuhuku, D.** A study of the One-path Deep Drawing Spinning of Cups, *Journal of Materials Processing Technology*, 2005, **159**, 397-400;
- [17] **Wang, Q., Wang, T., and Wang, Z. R.** A Study of the Working Force in Conventional Spinning, *Proceedings of the Forth International Conference of Rotary Forming*, October 17-21, 1989, pp. 103-108;
- [18] **Arai, H.** Robotic Metal Spinning – Shearing Spinning Using Force Feedback Control, *Proceedings of 2003 IEEE, International Conference on Robotics & Automation*, 2003, Taipei, Taiwan;
- [19] **Hayama, M.** Study on Spinnability of Aluminium and its Alloys, *Bulletin of the Faculty of Engineering*, Yokohama National University, 1981, **30** , 63-72;
- [20] **Quigley, E. and Monaghan, J.** An Analysis of Conventional Spinning of Light Sheet Metal. *International Conference on Sheet Metal 1999*;

- [21] **Wang, L., Long, H., Ashley, D., Roberts M., and White, P.** Analysis of single-pass conventional spinning by Taguchi and Finite Element methods. *Special Edition of Steel Research International*, Verlag Stahleisen GmbH, 2010, 81, 974-977;
- [22] **Wang L. and Long, H.** Stress analysis of multi-pass conventional spinning. *The 8th International Conference on Manufacturing Research*, Durham, UK, 2010, pp. 186-191;
- [23] **Finckenstein, E. von and Dierig, H.** CNC-Drücken, *Annals of the CIRP*, 1990, **39/1**, 267-270;
- [24] **Köhne, R.** Rechnergestützte Ermittlung und Verarbeitung von Umformparametern für das Fertigungsverfahren Drücken. PHD-Thesis, Dortmund University, 1984 (in German).